Electronic Supplementary Material (ESI) for Materials Chemistry Frontiers.
This journal is © the Partner Organisations 2022

Polar Side-Chain Tuning of Perylene Diimide and Fluorene-Based Cathode Interfacial Material for High-Performance Inverted Perovskite Solar Cells

Tao Wu,[a] Daizhe Wang,[a] Xingjian Jiang,[a] Xianxian Ge,[a] Fengyun Guo,[a] Tengling Ye,[b,] Shiyong Gao,[a] Yong Zhang[a,c*]*

[a]School of Materials Science and Engineering, Harbin Institute of Technology, Harbin 150001, China

[b]School of Chemistry and Chemical Engineering, Harbin Institute of Technology, Harbin 150001, China

[c]School of Materials Science and Engineering, Zhengzhou University, Zhengzhou 450001, China

Email: yongzhang@hit.edu.cn; ytl@hit.edu.cn

Experimental Procedures

1. Materials

All chemicals and solvents were purchased from commercials and used directly without further purification except mention.

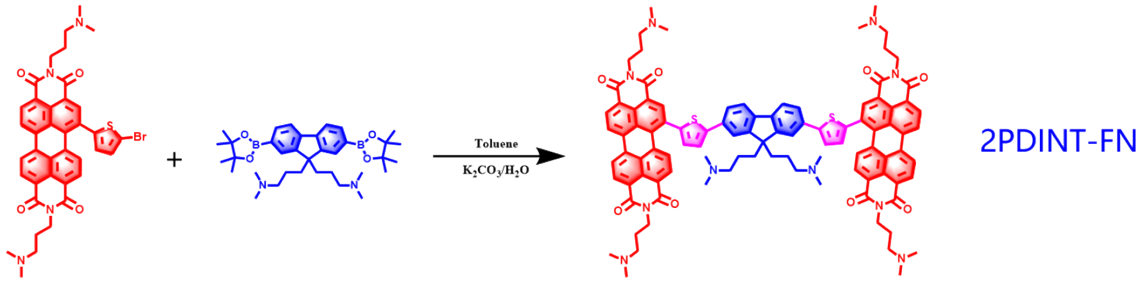

Scheme S1. Synthetic route of 2PDINT-FN

Synthesis of compound 2PDINT-FN

PDINT-Br (866.0 mg, 1.2 mmol), 2,7-dibromo-9,9- bis(3′-(N,N-dimethylamino)propyl) fluorene (248 mg, 0.5 mmol), tetrakis(triphenylphosphine)palladium [$(PPh_3)_4Pd$] (20 mg), and several drops of Aliquat 336 were dissolved in a mixture of 5 mL of toluene and 1 mL of 2 M Na_2CO_3 aqueous solution. The mixture was refluxed with vigorous stirring for 12 h under an argon atmosphere. After the solvent was removed with rotary evaporator to obtain crude product. The product was then further purified by column chromatography on silica gel using DCM: Methanol:Triethylamine (50: 1: 1) as eluent afford a dark red solid (1.4 g, 87%). ^{1}H NMR (500 MHz, CDCl3, δ): 8.6-8.8 (m, 8H), 8.4-8.5 (m, 2H), 8.2-8.3(m, 8H), 7.7-7.9 (m, 2H), 7.6-7.7 (d, 4H), 5.3-5.4 (m, 8H), 3.3-3.4 (m, 12H), 2.9-3.1 (s, 36H), 1.7-1.8 (m, 4H), 1.2-1.3 (m, 12H). ^{13}C NMR (CDCl3, δ): 163.7, 163.5, 163.4, 161.4, 148.2, 141.5, 140.5, 139.7, 137.9, 137.0, 136.4, 132.2, 131.4, 131.1, 130.8, 129.6, 129.5, 129.4, 128.8, 128.2, 127.5, 126.2, 123.9, 123.8, 122.7, 63.5, 58.7, 58.0, 57.2, 53.0, 45.4, 45.2, 44.9, 26.0, 25.6, 22.8. HRMS: calculated for $C_{99}H_{96}N_{10}O_8S_2$, 1617.69, found 1619.03.

2. Material characterizations

^{1}H NMR spectra were measured on a Bruker-AV 500MHz with d-chloroform as the solvent and trimethylsilane as the internal reference. UV-visible absorption spectra were measured via Beijing Purkinje General-TU-1901 spectrophotometer. Cyclic voltammetry （come from our research group）was performed on a CH Instruments CHI660E electrochemical workstation with a three-electrode system in 0.1 M PF_6 acetonitrile solution at a scan rate of 40 mV/s. ITO with sample film was used as the working electrode. A Pt wire was used as the counter electrode and Ag/AgCl was used as the reference electrode. Ferrocene/ferrocenium redox couple was used as the external standard and its redox potential is 0.36 V vs. Ag/AgCl. The LUMO energy levels were calculated from the onset

of the reduction potentials using the following equations: E_{HOMO} = -e (φ_{red} + 4.44) (eV); E_{LUMO}= E_{opt}^{g}+E_{HOMO} (eV). Atomic force microscopy (AFM) images were obtained using a NanoMan VS microscope in the tapping mode. SEM images were obtained with Merlin Compact. ESR (State Key Laboratory of Luminescent Materials and Devices, South China University of Technology) spectra were recorded on a JEOL JES-FA200 ESR spectrometer (300 K, 9.063 GHz, X-band). The steady-state PL spectra was performed by a He–Cd ultraviolet laser at 405 nm using Micro-PL Spectrometer-Lab-RAM HR800. UPS (PHI CHINA) images were obtained using a PHI5000 Versa Probe III (X-ray source: Al Kα mono (1486.6 eV)).

3. Device fabrication and characterization

The etched ITO glass was rinsed with deionized water and followed by ultrasonic cleaning with acetone and isopropanol twice. Then, ITO substrates were treated with oxygen plasma for 10 mins. Afterward, 3.5 mg PTAA and 2 mg Tris(pentafluorophenyl)borane (BCF) were dissolved in 1 mL chlorobenzene (CB), respectively. After the solutes were completely dissolved, 12wt% of BCF was added into the PTAA solution. The BCF-PTAA solution was illuminated for 5 mins under solar simulator (100 mW·cm^{-2}) and was kept in the dark at room temperature, waiting to be used. PTAA films were spin-coated at 4500 rpms for 25 secs, followed by annealing at 120 ℃ for 10mins. The perovskite light absorption layer was prepared by the following typical one-step method. ($FAPbI_3$: $MAPbBr_3$=83:17 was dissolved in VDMF: VDMSO = 5:1, and CsI 5% was added) was spin-coated on the 1.1 × 1.5 cm^2 ITO/PTAA substrate at 5000 rpm for 35 s. After 10 s, 300 μL of anisole is dispensed on the sample. Then, the samples were annealed at 110 ºC for 30 mins. After cooling down to room temperature, a 15mg/mL $PC_{61}BM$ solution in CB

was spin-coated at 1500 rpms for 60s. Then 0.5-1.0mg/ mL 2PDINT-FN or 2PDINT-FN(+) (dissolved in 2,2,2-trifluoroethanol) was spin-coated on $PC_{61}BM$ at 2500 rpms for 1 min. Lastly, 100 nm Ag film was thermally evaporated as a counter electrode under a pressure of 7×10^{-4} Pa, and the active area of the device was 0.04 cm^2. Complete fabrication process of PVSCs was done in the glovebox.

The electron-only devices for 2PDINT-FN and 2PDINT-FN (+) films were fabricated as follows. The1.5 M ZnO precursor solution was spin-coated on the cleaned ITO at 4000 rpm for 30 s and then annealed at 250 °C for 30 min. After the films were cooled down, the 15 mg mL^{-1} 2PDINT-FN or 2PDINT-FN (+) (2,2,2-trifluoroethanol solution) was spin-coated at 1500 rpm for 60 s without additional annealing. Finally, Ca(20 nm) and Al (100 nm) films were evaporated on top of the active layer as the electrode.

The mobility was determined by fitting the dark current to the model of a single carrier SCLC, which is described by the equation:

$$J = \frac{8}{9}\varepsilon_0\varepsilon_r\mu_h\frac{V^2}{d^3}$$

Where J is the current, μ_h is the zero-field mobility, ε_0 is the permittivity of free soace, ε_r is the relative permittivity of the material, d is the thickness of the active layer, and V is the effective voltage.

Conductivity measurements were performed by measuring *J-V* characteristics between ITO and Ag electrodes using a Keithley 2400 source Measure Unit. Also, 2PDINT-FN or 2PDINT-FN (+) (2,2,2-trifluoroethanol solution) was spin-coated on the patterned ITO glass. Then Ag (100 nm) films were evaporated on top of the active layer as the electrode.

The conductivity (σ) was calculated by the following equation σ= W/(RLD), where L was the channel length with 2.6 mm, W was the channel width 2.0 mm, D was the thickness of PDI-2N or PDI-4N film measured by AFM, and R was the film resistance derived from the slope of the *J-V* curves.

Trap density was studied with an architecture of ITO/SnO2/perovskite/PC61BM/CIL/ Ag and described by using equation:

$$N_{traps}= \frac{2\varepsilon_0\varepsilon_r V_{TEF}}{eL^2}$$

where V_{TFL} is the onset voltage of the trap-filled limit region, *e* is the elemental charge, and *L* is the distance between the electrodes.

The hysteresis of the J–V curves for PVSCs with different CIL was evaluated by using a hysteresis index (HI), which is determined by the following equation：

$$HI= \frac{PCE_{reverse} - PCE_{forward}}{PCE_{reverse}}$$

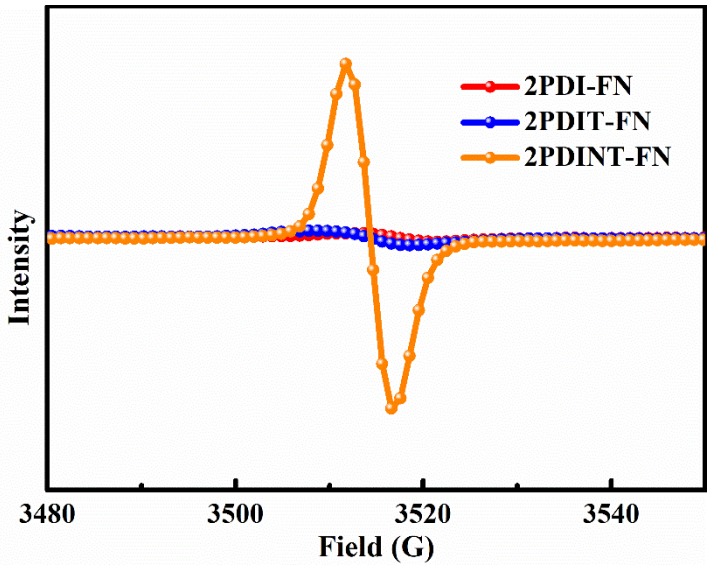

Fig. S1 Electron spin resonance (ESR) of 2PDI-FN, 2PDIT-FN and 2PDINT-FN in films.

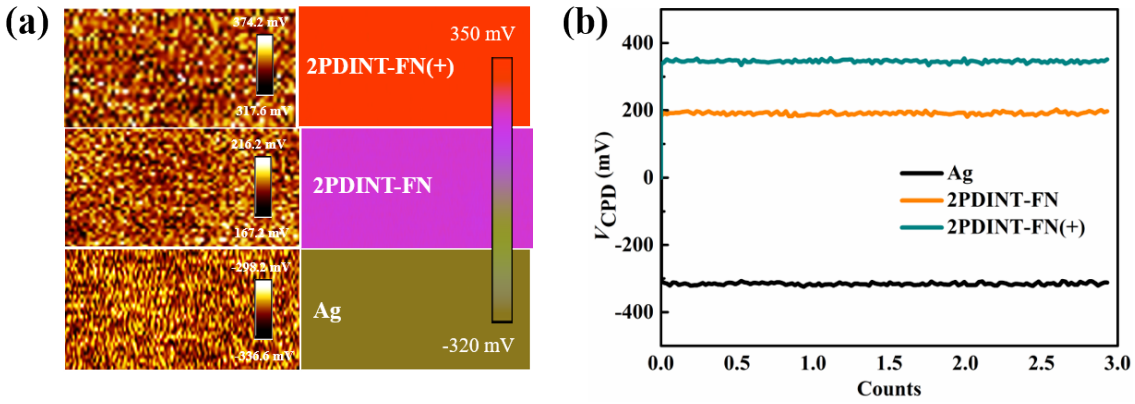

Fig. S2 Surface potential maps from KPFM measurements for bare Ag, 2PDINT-FN/Ag, 2PDINT-FN(+)/Ag.

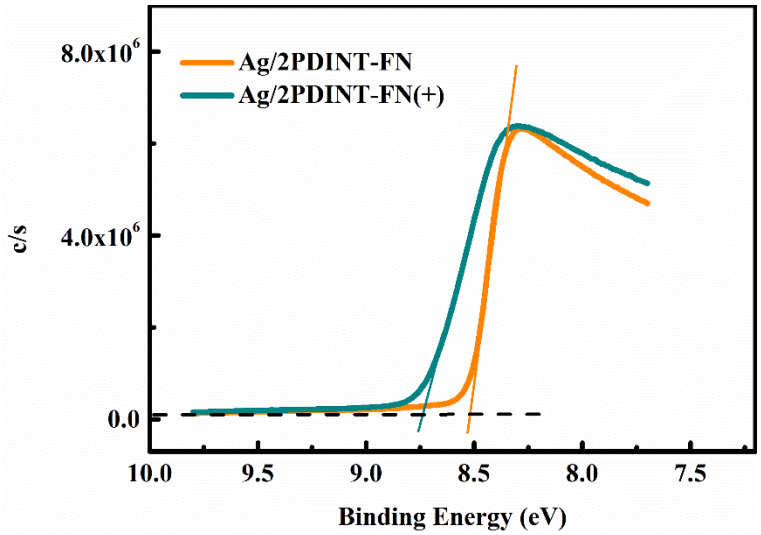

Fig. S3 UPS of 2PDINT-FN/Ag and 2PDINT-FN(+)/Ag film.

Table S1 Comparison of the physicochemical properties of the CIM of 2PDINT-FN and 2PDINT-FN(+).

CIMs	λ_{max} (nm)	λ_{edg} (nm)	HOMO (eV)	LUMO (eV)	E_g (eV)	Conductivity (10^{-2} S cm^{-1})	μ ($(10^{-3}cm^2V^{-1}s^{-1})$)
2PDINT-FN	381	774	-5.65	-4.06	1.60	1.32	1.09
2PDINT-FN(+)	380	789	-	-	1.57	1.91	3.87

Table S2 Photovoltaic parameters of PSCs with 2PDINT-FN or 2PDINT-FN(+) as the ETLs.

CILs	V_{OC} (mV)	J_{sc} (mA cm^{-2})	FF (%)	PCE (%)
2PDINT-FN-reverse	1173	23.98	71.21	20.03
2PDINT-FN-forward	1171	24.08	68.81	19.40
2PDINT-FN(+)-reverse	1178	25.06	74.00	21.85
2PDINT-FN(+)-forward	1174	25.10	72.96	21.51

Table S3 The PCE with different CIMs for inverted perovskite solar cells in recent years.

Device structure	J_{sc} [mA cm^{-2}]	V_{oc} [V]	FF [%]	PCE [%]	Ref.
ITO/PEDOT:PSS/ perovskite /t-BPTI/C_{60}/BCP/Al	19.80	0.97	60.55	11.63	[1]
ITO/P3CT-Na/ perovskite /TPE-PDI4/C_{60}/BCP/Ag	21.98	1.05	81	18.78	[2]
ITO/P3CT-Na/perovskite/Tr-PDI3/C_{60}/BCP/Ag	22.22	1.08	83	19.83	[3]
ITO/TiO2/PDI_2/ perovskite /Spiro-OMeTAD/Ag	23.29	1.07	79.61	19.84	[4]
ITO/PTAA:F4-TCNQ/PMMA/ perovskite /IDTT2FPDI/ PCBM/ Bphen/Al	23.9	1.10	73.8	19.4	[5]
ITO/LT-NiO/ perovskite /PCBM/PDINO/Ag	20.57	1.11	76.5	17.5	[6]
ITO/PEDOT:PSS/ perovskite /NDI-PhE/Al	23.1	1.10	80.8	20.5	[7]
ITO/PTAA/perovskite /PCBM/ C_{60}/ BCP/Al	22.6	1.13	75	19.4	[8]
ITO/NiOx/perovskite /PCBM/$Ca(acac)_2$/Ag	23.45	1.08	79	20.15	[9]
ITO/PTAA:F4-TCNQ/PMMA /perovskite /PCBM/ Bphen/Al	22.59	1.114	73.93	18.61	[10]
ITO/PTAA:F4-TCNQ/PMMA /perovskite /PCBM/ QAPDI/Al	23.87	1.130	76.18	20.55	[10]
ITO/PTAA / perovskite /P(BTI-PDI)/ BCP/Ag	23.3	1.12	79.1	20.8	[11]
ITO/PTAA / perovskite /PBTzTI/ BCP/Ag	22.94	1.136	80.1	20.86	[12]
FTO/ NiO_x/perovskite /PCBM/ C_{60}MPE-ionene/Ag	22.15	1.10	79.15	19.28	[13]
ITO/P3CT-Na / perovskite /PC-2/ C_{60}/BCP/Ag	22.49	1.11	0.821	20.50	[14]
ITO/PTAA / perovskite /PIL/ C60/BCP/Cu	22.54	1.158	81.93	21.39	[15]
ITO/PTAA:BCF/ perovskite /PC_{61}BM/	22.73	1.153	80.56	21.06	[16]

PDI-T/Ag					
ITO/PTAA:BCF/ perovskite /$PC_{61}BM$/ 2PDINT-FN/Ag	1173	23.98	71.21	20.03	This work
ITO/PTAA:BCF/ perovskite /$PC_{61}BM$/ 2PDINT-FN(+)/Ag	1178	25.06	74.00	21.85	This work

It can be seen from the above table that the device performance of 2PDINT-FN(+) is highly competitive as a cathode interface material, and it is the highest value of PCE in inverted perovskite solar cells with PDI-base interlayer materials as the cathode interlayer.

References

1. Karuppuswamy, P.; Chen, H.-C.; Wang, P.-C.; Hsu, C.-P.; Wong, K.-T.; Chu, C.-W., The 3 D Structure of Twisted Benzo[Ghi]Perylene-Triimide Dimer as a Non-Fullerene Acceptor for Inverted Perovskite Solar Cells. *ChemSusChem* **2018**, *11*, 415-423.
2. Jiang, K.; Wu, F.; Yu, H.; Yao, Y.; Zhang, G.; Zhu, L.; Yan, H., A Perylene Diimide-Based Electron Transport Layer Enabling Efficient Inverted Perovskite Solar Cells. *J. Mater. Chem. A* **2018**, *6*, 16868-16873.
3. Wang, R.; Jiang, K.; Yu, H.; Wu, F.; Zhu, L.; Yan, H., Efficient Inverted Perovskite Solar Cells with Truxene-Bridged Pdi Trimers as Electron Transporting Materials. *Mater. Chem. Front.* **2019**, *3*, 2137-2142.
4. Yang, L.; Wu, M.; Cai, F.; Wang, P.; Gurney, R. S.; Liu, D.; Xia, J.; Wang, T., Restrained Light-Soaking and Reduced Hysteresis in Perovskite Solar Cells Employing a Helical Perylene Diimide Interfacial Layer. *J. Mater. Chem. A* **2018**, *6*, 10379-10387.
5. Wang, H.; Yang, F.; Xiang, Y.; Ye, S.; Peng, X.; Song, J.; Qu, J.; Wong, W.-Y., Achieving Efficient Inverted Perovskite Solar Cells with Excellent Electron Transport and Stability by Employing a Ladder-Conjugated Perylene Diimide Dimer. *J. Mater. Chem. A* **2019**, *7*, 24191-24198.
6. Hou, Y., et al., Overcoming the Interface Losses in Planar Heterojunction Perovskite-Based Solar Cells. *Adv. Mater.* **2016**, *28*, 5112-5120.
7. Jung, S.-K., et al., Homochiral Asymmetric-Shaped Electron-Transporting Materials for Efficient Non-Fullerene Perovskite Solar Cells. *ChemSusChem* **2019**, *12*, 224-230.
8. Shao, Y.; Yuan, Y.; Huang, J., Correlation of Energy Disorder and Open-Circuit Voltage in Hybrid Perovskite Solar Cells. *Nat. Energy* **2016**, *1*, 15001.
9. Zhao, Z. Q.; You, S.; Huang, J.; Yuan, L.; Xiao, Z. Y.; Cao, Y.; Cheng, N.; Hu, L.; Liu, J. F.; Yu, B. H., Molecular Modulator for Stable Inverted Planar Perovskite Solar Cells with Efficiency Enhanced by Interface Engineering. *J. Mater. Chem. C* **2019**, *7*, 9735-9742.
10. Wang, H.; Song, J.; Qu, J.; Lian, J.; Qian, P.-C.; Wong, W.-Y., A Novel Perylene Diimide-Based Zwitterion as the Cathode Interlayer for High-Performance Perovskite Solar Cells. *J. Mater. Chem. A* **2020**, *8*, 18117-18124.
11. Shi, Y., et al., Imide-Functionalized Acceptor–Acceptor Copolymers as Efficient Electron Transport Layers for High-Performance Perovskite Solar Cells. *J. Mater. Chem. A* **2020**, *8*, 13754-13762.

12. Chen, W.; Shi, Y.; Wang, Y.; Feng, X.; Djurišić, A. B.; Woo, H. Y.; Guo, X.; He, Z., N-Type Conjugated Polymer as Efficient Electron Transport Layer for Planar Inverted Perovskite Solar Cells with Power Conversion Efficiency of 20.86%. *Nano Energy* **2020**, *68*, 104363.
13. Zheng, T.; Zhou, H.; Fan, B.; Zhao, Y.; Jin, B.; Fan, L.; Peng, R., Designing Conductive Fullerenes Ionene Polymers as Efficient Cathode Interlayer to Improve Inverted Perovskite Solar Cells Efficiency and Stability. *Chemical Engineering Journal* **2021**, *415*, 128816.
14. Jia, J.; Wu, F.; Zhu, L.; Yang, C., Unfused Electronic Acceptor-Based Polymers as Interfacial Materials for Efficient Inverted Perovskite Solar Cells. *ACS Appl. Mater. Interfaces* **2021**, *13*, 33328-33334.
15. Caprioglio, P., et al., Bi-Functional Interfaces by Poly(Ionic Liquid) Treatment in Efficient Pin and Nip Perovskite Solar Cells. *Energy Environ. Sci.* **2021**, *14*, 4508-4522.
16. Wu, T.; Wang, D.; Lu, Y.; Zheng, Z.; Guo, F.; Ye, T.; Gao, S.; Zhang, Y., Multifunctional Perylenediimide-Based Cathode Interfacial Materials for High-Performance Inverted Perovskite Solar Cells. *ACS Appl. Energy Mater.* **2021**, *4*, 13657-13665.